

Journal of Biomedical Optics

SPIEDigitalLibrary.org/jbo

Reduction of shading-derived artifacts in skin chromophore imaging without measurements or assumptions about the shape of the subject

Kenichiro Yoshida
Izumi Nishidate
Nobutoshi Ojima
Kayoko Iwata

Reduction of shading-derived artifacts in skin chromophore imaging without measurements or assumptions about the shape of the subject

Kenichiro Yoshida,^{a,*} Izumi Nishidate,^b Nobutoshi Ojima,^a and Kayoko Iwata^a

^aKao Corporation, Beauty Research Center, 2-1-3 Bunka, Sumida-ku, Tokyo 131-8501, Japan

^bTokyo University of Agriculture & Technology, Graduate School of Bio-applications & Systems Engineering, 2-24-16 Naka-cho, Koganei, Tokyo 184-8588, Japan

Abstract. To quantitatively evaluate skin chromophores over a wide region of curved skin surface, we propose an approach that suppresses the effect of the shading-derived error in the reflectance on the estimation of chromophore concentrations, without sacrificing the accuracy of that estimation. In our method, we use multiple regression analysis, assuming the absorbance spectrum as the response variable and the extinction coefficients of melanin, oxygenated hemoglobin, and deoxygenated hemoglobin as the predictor variables. The concentrations of melanin and total hemoglobin are determined from the multiple regression coefficients using compensation formulae (CF) based on the diffuse reflectance spectra derived from a Monte Carlo simulation. To suppress the shading-derived error, we investigated three different combinations of multiple regression coefficients for the CF. *In vivo* measurements with the forearm skin demonstrated that the proposed approach can reduce the estimation errors that are due to shading-derived errors in the reflectance. With the best combination of multiple regression coefficients, we estimated that the ratio of the error to the chromophore concentrations is about 10%. The proposed method does not require any measurements or assumptions about the shape of the subjects; this is an advantage over other studies related to the reduction of shading-derived errors. © The Authors. Published by SPIE under a Creative Commons Attribution 3.0 Unported License. Distribution or reproduction of this work in whole or in part requires full attribution of the original publication, including its DOI. [DOI: [10.1117/1.JBO.19.1.016009](https://doi.org/10.1117/1.JBO.19.1.016009)]

Keywords: visible light spectroscopy; imaging; chromophore concentration; multiple regression analysis; shading; melanin; hemoglobin.

Paper 130613RR received Aug. 21, 2013; revised manuscript received Dec. 8, 2013; accepted for publication Dec. 9, 2013; published online Jan. 9, 2014.

1 Introduction

The concentrations of chromophores in skin provide important information for making a diagnosis, and images can provide additional information, such as the size of a lesion, that aid visual understanding. Therefore, many studies have been conducted to evaluate the concentration of chromophores,¹⁻⁶ and some of these studies discuss imaging, in which visible light spectroscopy is usually used to achieve high spatial resolution.⁷⁻¹³ Multiple regression analysis (MRA) based on the Beer-Lambert (B-L)³ law is a simple way to correlate the chromophore concentrations with the reflectance of skin. The B-L law has been applied to the three-layer skin model of epidermis, dermis, and fat, with the assumptions that no scattering occurs in the epidermis or dermis and no wavelength dependency exists in the reflectance from the fat layer.³ With these assumptions, the optical path length becomes constant and does not depend on wavelength. Therefore, in accordance with the B-L law, the absorbance (the logarithm of the inverse of the reflectance) can be expressed as a linear combination of the absorption coefficient spectrums of melanin, oxygenated hemoglobin, and deoxygenated hemoglobin, and a constant term. The constant term comes from the reflectance of the fat layer. The regression analysis uses the absorbance spectrum as a response variable and the extinction coefficient of each

of the chromophores as the predictor variables. Although the implementation is easy, the model is quite different from actual conditions, and it leads to inconsistencies between the actual and the fitted spectrums.^{4,14,15}

To improve the estimation, the modified B-L method has been introduced.^{4,5} Although the method is based on the B-L law, the optical path length is allowed to be wavelength dependent. This added degree of freedom allows a part of the scattering effect to be included, and it improves the coefficient of determination.^{4,5} In this method, as the predictor variables in the MRA, the product of each absorption coefficient and the wavelength-dependent path length was used. However, the method assumes that the optical path length is independent of the concentrations of chromophores, and thus the results are still different from measurements of the actual phenomenon. Neither the nonlinearity between the concentration and the absorbance nor the cross-talk between the chromophores has been taken into account.^{1,14,15}

In order to fully account for the effect of scattering in the estimation of chromophore concentrations, several methods have been considered; these include methods based on random work theory,¹² Kubelka-Munk theory,⁸ a support vector machine,¹¹ and an empirical method aided by a Monte Carlo simulation (MCS).^{1,9} Although scattering effects are fully considered in these methods, the methods are susceptible to shading-derived errors caused by the incomplete estimation of the irradiance.^{8,11,12} This is a serious problem for visual understanding and quantitative evaluation of the chromophore imaging.

*Address all correspondence to: Kenichiro Yoshida, E-mail: yoshida.kenichiro@kao.co.jp

Here, “shading” is the spatial distribution of irradiance. Shading results from the incident angle of the light, the spectral radiant intensity of the light source, and the distance from the light source. If the actual irradiance on the surface of a subject is lower than the estimate, then the apparent reflectance decreases and the chromophore concentrations will be overestimated; this tends to occur on the fringe areas of the subject. Therefore, for a precise calibration of reflectance, besides the radiant intensity distribution of the light, the shape of the subject also must be assessed (unless the areas of interest are limited to small, flat areas in which the irradiance can be fully assessed).¹ The problem with shading is common among methods that consider nonlinear scattering effects in imaging.¹⁰

Several studies have attempted to correct for the shading effect. In these studies, the shape of each subject was measured^{13,16} or the curvature effect was otherwise extracted¹² and taken into account. However, these approaches require hardware modifications and additional measurements or else assumptions about the shapes of the samples.

Incidentally, in the simple and modified B–L methods, in which the absorbance is expressed as a linear combination of each chromophore component with a constant term, the shading-derived error is not observed in the images of chromophore concentrations. The effect of surface curvature is proportional to irradiance, and in the absorbance, it is a constant term, independent of wavelength. Therefore, the effect of surface curvature will appear only in the constant term and will not appear in the image of the chromophore concentrations.

In order to fully account for the scattering effect and to reduce the shading-derived artifact, we propose an approach based on the MCS-aided empirical method.^{1,9} In this method, the simple B–L method is used to derive multiple regression coefficients related to the concentrations of melanin, oxygenated hemoglobin, and deoxygenated hemoglobin. Then, the multiple regression coefficients are converted to the concentrations of melanin and total hemoglobin (sum of oxygenated and deoxygenated hemoglobin) using compensation formulae (CF), which are derived from the diffuse reflectance spectra of human skin, numerically calculated in advance by a MCS.¹⁷ In the previous method,^{1,9} the constant term of the multiple regression coefficients, as well as the regression coefficients of melanin and total hemoglobin, were used in the CFs. Although the use of the constant term is important for estimating the absolute values of chromophore concentrations, it can cause the shading-derived error in reflectance that results in an overestimation of the chromophore concentrations. Since the shading-derived error is concentrated into the constant term during the first step of the MRA, selecting the optimal combination of multiple regression coefficients has the potential to satisfy both of the requirements. *In vivo* experiments with a human forearm were performed to confirm the usefulness of the proposed approach for improving the robustness of the method against the estimation error in the irradiance.

2 Materials and Methods

2.1 Outline of the Method

According to the B–L law, the absorbance spectrum $A(\lambda)$, which is derived from the reflectance spectrum $R(\lambda)$ as $A(\lambda) = \log(1/R(\lambda))$, can be approximated with the following formula:^{1,9}

$$A(\lambda) = a_m \cdot \varepsilon_m(\lambda) + a_{oh} \cdot \varepsilon_{oh}(\lambda) + a_{dh} \cdot \varepsilon_{dh}(\lambda) + a_0. \quad (1)$$

Here, melanin, oxygenated hemoglobin, and deoxygenated hemoglobin are assumed to be the main contributors to the absorption of light in skin. In Eq. (1), λ represents the wavelength; ε_m , ε_{oh} , and ε_{dh} are the spectral absorption coefficients of melanin, oxygenated hemoglobin, and deoxygenated hemoglobin, respectively; a_m , a_{oh} , and a_{dh} are the respective concentration-related values; and a_0 is the constant term. Equation (1) can be calculated by a multiple regression analysis (MRA1), in which A represents the response variables, and ε_m , ε_{oh} , and ε_{dh} are the predictor variables. Then, a_m , a_{oh} , a_{dh} , and a_0 are derived as the multiple regression coefficients.

Our proposed method obtains prior estimates of the relationship between the MRA1 regression coefficients and the chromophore concentrations of the MCS. With the MCS, a spectrum can be calculated from a given set of chromophore concentrations according to the skin model described in Sec. 2.2. Then, a set of regression coefficients can be derived from the spectrum using MRA1. By calculating regression coefficients for several sets of concentrations, sets of regression coefficients can be associated with particular chromophore concentrations. Polynomial, exponential, or logarithmic functions, or a combination of these functions, can be used as the form of the CFs. In this study, we used a polynomial form because it can be solved analytically by MRA. To derive the CFs for calculating the concentrations from the regression coefficients, another multiple regression analysis (MRA2) was used. Here, we considered the original concentrations from the MCS to be the response variables and their products with the regression coefficients from MRA1 to be the predictor variables; we will call this MRA2. In symbolic form, MRA2 is expressed as

$$c_i = \vec{b}_i \cdot \vec{a}, \quad (2)$$

where i represents m (for melanin) or th (for hemoglobin). Here, c_i is the estimated concentration of the respective chromophore, \vec{a} is a vector whose elements are the regression coefficients from MRA1 and their higher-order terms, and \vec{b}_i is the vector converting the regression coefficients to concentrations.

2.2 Correlating the Multiple Regression Coefficient with the Chromophore Concentrations

We used the same skin model and the same parameters that were used in the previous studies^{1,9} as follows: a two-layered model of the epidermis with uniform melanin and an underlying dermis with uniform oxygenated and deoxygenated hemoglobin was used; the thicknesses of the epidermis and dermis were 0.06 and 4.94 mm, respectively. The refractive indices n were assumed to be 1.4, independent of wavelength and layer. The refractive index of the external area was set to 1. The absorption coefficients of the epidermis and dermis were assumed to be $\varepsilon_m(\lambda)C_m$ and $\varepsilon_{oh}(\lambda)C_{oh} + \varepsilon_{dh}(\lambda)C_{dh}$, respectively. Here, C_m , C_{oh} , and C_{dh} are the concentrations of melanin, oxygenated hemoglobin, and deoxygenated hemoglobin in each layer. For $\varepsilon_m(\lambda)$, we used the average absorption coefficient of a monomer melanosome with a concentration of 1 mol/l; this was approximated as $6.6 \times 10^{11} \times \lambda^{-3.33}$, where the unit of λ is nanometers.¹⁸ For ε_{oh} and ε_{dh} , we used the extinction coefficients of oxygenated and deoxygenated hemoglobin, respectively, converted to

the concentration of 45 hematocrit in blood.¹⁹ The scales of C_m , C_{oh} , and C_{dh} were the ratios of the concentrations to those under which $\epsilon_m(\lambda)$, $\epsilon_{oh}(\lambda)$, and $\epsilon_{dh}(\lambda)$, respectively, were derived. To characterize the scattering, a reduced scattering coefficient $\mu'_s(\lambda)$ is required; this is derived from $\mu'_s(\lambda) = \mu_s(\lambda) \times (1 - g)$, using the scattering coefficient $\mu_s(\lambda)$ and anisotropy g , which are the primitive parameters of scattering.^{20,21} The value of $\mu'_s(\lambda)$ for both the epidermis and dermis was $2 \times 10^5 \times \lambda^{-1.5} + 2 \times 10^{12} \times \lambda^{-4}$; the first term represents Mie scattering, the second one represents Rayleigh scattering,²⁰⁻²² and the unit of λ is nanometers.

The MCS (using the program MCML¹⁷) was used to derive the spectra for various concentrations of chromophores; a_m , a_{oh} , a_{dh} , and a_0 were then calculated using MRA1. The calculated melanin concentrations C_m were set from 1% to 10% in 1% intervals, the hemoglobin concentration C_{th} ($= C_{oh} + C_{dh}$) was set from 0.2% to 1% in 0.2% intervals, and the oxygen saturation C_{StO_2} ($= C_{oh}/C_{th}$) was set from 0% to 100% in 20% intervals. The wavelength was set from 500 to 600 nm in 20-nm intervals, and the number of photons under a single condition was 10^5 .²³ From the MCS calculations under the various conditions, a total of 300 spectra were generated. In the MCS, the incident angle was set to 0 deg and, for statistical accuracy, the reflectance was integrated over the entire reflected angle. Although the outgoing angle was not the same as in the actual measurement condition (see Sec. 2.6), it is appropriate if Lambertian reflection is assumed; it gives a first-order approximation of internal reflection.²⁴ For each combination of (C_m, C_{oh}, C_{dh}) , after the reflectance spectra were converted to absorbance spectra, a_m , a_{oh} , a_{dh} , and a_0 were calculated using MRA1.

2.3 Shading Effect

Shading has an effect on the results of MRA1, and thus consequently, on the estimated chromophore concentrations. Assuming Lambertian reflection and using θ_i to denote the angle between the surface and the incoming light, the irradiance is $\cos \theta_i$ times that of normal incidence, independent of wavelength. Therefore, the apparent reflectance can be expressed as $R' = R \times \cos \theta_i$, where the actual reflectance is defined as R . Also, the apparent absorbance A' can be expressed as $A' = \log(1/R') = A + \log(1/\cos \theta_i)$, where the actual absorbance is $A = \log(1/R)$. Since the second term is independent of the wavelength, a_0 becomes $\log(1/\cos \theta_i)$ larger than it is in the case of normal incidence.¹⁰

We assumed that a light, a camera, and a cylindrical subject of radius r are arranged as follows. The cylinder is placed so that the center is at the origin and the axis of symmetry lies along the x -axis, the camera lies on the z -axis, and the light source is in the xz -plane (Fig. 1). The light vector \vec{S} can be expressed as $(\sin \theta_s, 0, \cos \theta_s)$ at any point on the subject. Similarly, the normal vector \vec{N} at the point (x_0, y_0) is $(0, y_0/r, \sqrt{1 - y_0^2/r^2})$. Therefore, the incident angle (the angle between \vec{S} and \vec{N}) is $\cos^{-1}(\cos \theta_s \cdot \sqrt{1 - y_0^2/r^2})$. Under this arrangement, the incident angle depends on the y -coordinate and increases with increasing distance from the x -axis, so a_0 also increases. The intensity of the reflected light is expected to depend less on the viewing angle θ_o than on the incident angle, because, in the case of Lambertian reflection,²⁴ the observation point does not affect the intensity of the reflected light.

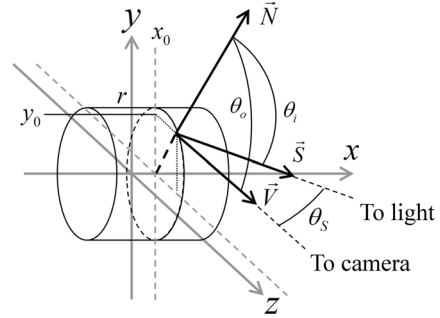


Fig. 1 Notation of positional and angular relationships for a point on a cylindrical subject in relation to a light source and a camera. Each symbol represents S : light vector, N : normal vector, V : viewing vector, θ_i : incident angle, θ_o : viewing angle, θ_s : angle between S and V , r : radius of the cylindrical subject, (x_0, y_0) : coordinate value of a point on the subject.

2.4 Formula of the Relationship Between the Multiple Regression Coefficients and the Chromophore Concentrations

From the description in Sec. 2.3, for MRA1, we assumed that the shading effect would appear mainly in the a_0 . Therefore, when using the regression coefficients of MRA1 to estimate the chromophore concentrations, removing a_0 from the CFs will eliminate the shading effect.

Note that the form of the polynomial equation is the key factor of our method. Removing a_0 from the CFs will reduce the estimated errors in the chromophore concentrations that are due to shading-derived errors in the reflectance. However, this will decrease the accuracy of the CFs, because a_0 also includes information related to the concentration of each chromophore. To compensate for the absence of a_0 , we separate a_{th} into a_{oh} and a_{dh} . To determine the appropriate CFs, we considered using the following three types of \vec{a} in Eq. (2) and examined each with various choices for the regression coefficients.

$$\vec{a}^{CF1} = (1 \ a_m \ a_{th} \ a_0 \ a_m^2 \ a_{th}^2 \ a_0^2 \ a_m \cdot a_{th} \ a_{th} \cdot a_0 \ a_0 \cdot a_m)^T \quad (3)$$

$$\vec{a}^{CF2} = (1 \ a_m \ a_{th} \ a_m^2 \ a_{th}^2 \ a_m \cdot a_{th} \ a_m^3 \ a_{th}^3 \ a_m \cdot a_{th}^2 \ a_m^2 \cdot a_{th})^T \quad (4)$$

$$\vec{a}^{CF3} = (1 \ a_m \ a_{oh} \ a_{dh} \ a_m^2 \ a_{oh}^2 \ a_{dh}^2 \ a_m \cdot a_{oh} \ a_{oh} \cdot a_{dh} \ a_{dh} \cdot a_m)^T \quad (5)$$

Here, a_{th} is defined as the sum of a_{oh} and a_{dh} , and T represents the transpose. In Eq. (3), a_m , a_{th} , and a_0 were used in the CFs, and the choice of the regression coefficient was the same as in previous studies.¹⁹ In Eq. (4), a_m and a_{th} were used in the CFs, but a_0 was not used. In Eq. (5), a_{oh} and a_{dh} were used instead of a_{th} . To adjust the degrees of freedom between CF1, CF2, and CF3, the maximum degree of CF2 was set to three, and those of CF1 and CF3 were set to two. In CF2 and CF3, in which a_0 was omitted, the artifact from shading was expected to be removed due to the manifestation of the shading effect in the coefficient a_0 (see Sec. 2.3). In any of these CFs, the oxygen saturation a_{StO_2} can be calculated as a_{oh}/a_{th} .

2.5 Experiments

2.5.1 Correlation between estimated and expected value of chromophore concentrations

The chromophore concentrations were estimated with each CF from the spectrum made by the MCS and compared with the inputs of the MCS, which were the expected values. For this calculation, the skin model described in Sec. 2.2 (the same skin model parameters used for MRA2) was used.

2.5.2 Measurement of forearm skin

The right forearms of Japanese males ($N = 5$) in their 20s to 40 s were measured with the measuring device described in Sec. 2.6. For each subject, the forearm was placed horizontally and images were captured. This was done for two different postures: the inner forearm facing front (angle 1) and facing ~ 45 deg upward (angle 2). To correlate the positions on the forearm, several points were marked in a reticular pattern at a distance of 2 cm from neighboring points. After performing MRA1, the chromophore concentrations were calculated as images by using the CFs.

The averaged values of the chromophore concentrations in a 10×10 pixel (2.5×2.5 mm² when the surface faces front) area at the middle of horizontally neighboring marks were calculated for each CF.

2.6 Measuring Device

The following apparatus was prepared (Fig. 2). A camera (CV-M7 + CL; jAi, Yokohama, Japan) was set in front of the subject. A liquid-crystal wavelength-tunable filter (VariSpec; CRi, Hopkinton, Massachusetts; full width at half maximum: 10 nm) and a polarizer were set in front of the camera. Two halogen lights were set at the left and right sides of the camera in such a way that the angle between the camera and the lights was 30 deg. An infrared cut filter and a polarizer, which was set to be orthogonal to the polarizer in front of the camera, were set between each light source and the subject; this was done to reduce the specular reflection from the skin surface.¹⁰

Images were captured using a personal computer and by varying the transparent wavelength of the VariSpec. The resolution of the camera was 4 pixel/mm on a subject facing frontwards, and the pixel depth was 10 bits. The transparent wavelength was set from 500 to 600 nm, with an interval of

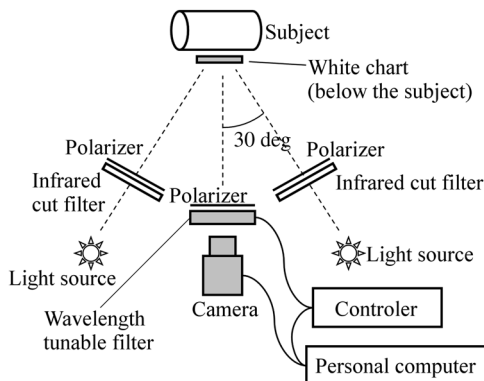


Fig. 2 Schematic of the measuring system.

20 nm. The measurement time was about 10 s in total. Although we used a color camera, we used only the green channel. For calibration, we captured images of a gray card besides images of subjects, and the pixel values were converted to reflectance in a pixel-by-pixel manner. In the calibration, the pixel value of the white chart was also used, and it was set below the subject. The reflectance can be derived from this calibration if the surface of interest is perpendicular to the line of sight. However, if the surface of interest is not perpendicular to the line of sight, the shading-derived error in the reflectance, i.e., the calibration error in the reflectance, will be increased according to $\cos \theta_i$, as shown in Fig. 1.

2.7 Statistics

2.7.1 Correlation between estimated and expected value of chromophore concentrations

In the statistical analysis of the estimated and expected values of chromophore concentrations from the MCS, the standard deviation, σ , of each condition was defined as

$$\sigma_i^2 = \sum_{j=1}^n (c_{i,j} - C_{i,j})^2 / (n - 1). \quad (6)$$

Here, i is m (melanin) or th (hemoglobin), n is the number of data points, j indicates a particular data point, and $c_{i,j}$ and $C_{i,j}$ are, respectively, the estimated and expected values.

2.7.2 Measurement of forearm skin

In the statistical analysis of forearm skin, the variance V was determined as

$$V_{i,j} = (c_i \text{ of angle 1 at } j' \text{ th area}) - (c_i \text{ of angle 2 at } j' \text{ th area}). \quad (7)$$

Here, i is m (melanin) or th (hemoglobin) and c_i is the measured chromophore concentration. Assuming that the dispersion of the difference between c_i and the real value is equal to half of the dispersion of V , the standard deviation σ_i of the difference between the real and measured values of c_i can be derived from the following equation:

$$\sigma_i^2 = \left(\sum_{j=1}^n V_{i,j}^2 / (n - 1) \right) / 2, \quad (8)$$

where n is the number of measured areas.

3 Results

3.1 Correlation between Estimated and Expected Value of Chromophore Concentrations

For CF1, CF2, and CF3, the relationships between the original C_i and the estimated c_i ($i = m, th$) are shown in Fig. 3. The σ were 0.025, 0.481, and 0.084 for the melanin concentration estimated with CF1, CF2, and CF3, respectively, and 0.008, 0.092, and 0.016 for the hemoglobin concentration measured with CF1, CF2, and CF3, respectively. The errors increased in the order of CF1, CF3, and CF2.

3.2 Measurement of Forearm Skin

Images of the inner forearm from sets of spectra images are shown in Fig. 4, and Fig. 5 shows the images of the regression coefficients of the framed area in Fig. 4(a). Although the systematic variation from the center to the fringe (upper and lower sides in the pictures) cannot be found in a_m [Fig. 5(a)] or a_{th} [Fig. 5(b)], the value of a_0 became greater at the fringe [Fig. 5(e)]. In a_{oh} [Fig. 5(c)] and a_{dh} [Fig. 5(d)], the values became slightly larger and smaller at the edges, respectively, but the degree to which this happens is smaller than it was for a_0 . The value of a_{SiO_2} was affected by the trend of a_{oh} and a_{dh} and decreased slightly at the fringe [Fig. 5(f)]. The average and standard deviation of each regression coefficient of the sites A, B, C, and D in Fig. 4(a) were calculated, and the values were as follows: $a_m = (2.1 \pm 0.2) \times 10^{-4}$; $a_{th} = (1.6 \pm 0.1) \times 10^{-6}$; $a_{oh} = (8.5 \pm 0.9) \times 10^{-7}$; $a_{dh} = (7.6 \pm 1.1) \times 10^{-7}$; $a_0 = (2.2 \pm 0.2) \times 10^{-1}$; and $a_{SiO_2} = (55 \pm 5)\%$.

Next, the chromophore concentrations were estimated with each CF. Figure 6 presents the images of a representative example of these. In CF1, the values of c_m and c_{th} increased from the center to the fringe, but in CF3, no such tendency could be observed. This tendency is also seen in Fig. 7. From the cross-section, the values of CF3 near the center were close to those of CF1 [Figs. 7(a) and 7(b)]. On the other hand, the fluctuations of CF3 are larger than those of CF1. In CF2 also, a systematic variation could not be found, but the fluctuations

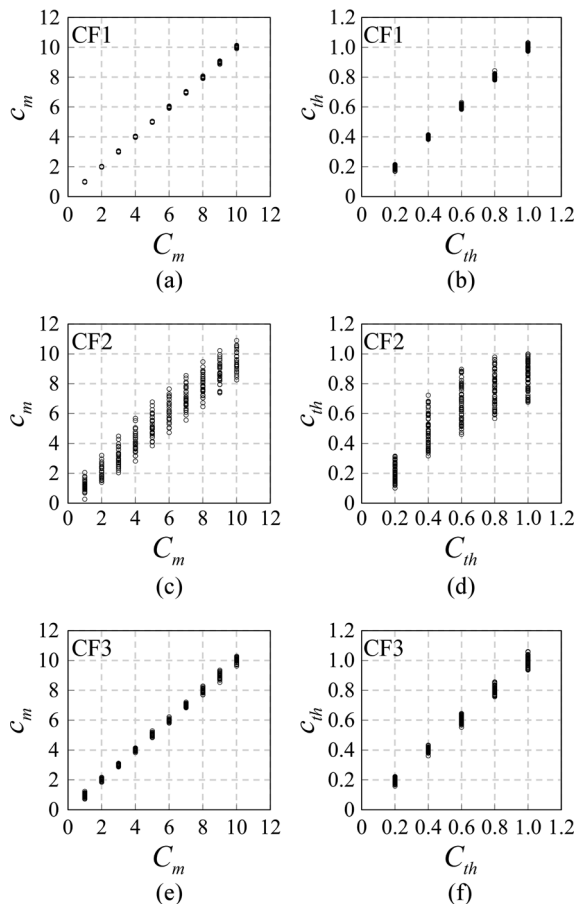


Fig. 3 Correlations between the original and the estimated values of (a) melanin and (b) hemoglobin, using CF1; (c) melanin and (d) hemoglobin, using CF2; and (e) melanin and (f) hemoglobin, using CF3. Horizontal axis: original values; vertical axis: estimated values. The unit of the horizontal and vertical axes is %.

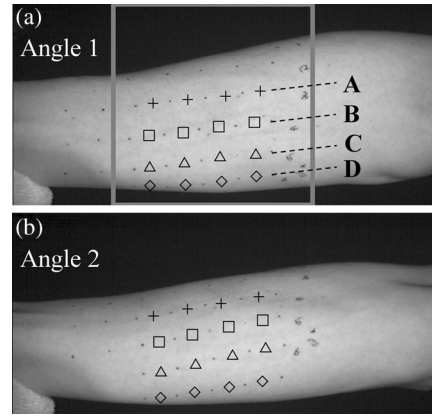


Fig. 4 Representative example of measured images (appearance) from different angles. The inner side of the forearm faced (a) straight or (b) upward. The hand is to the left side. To correlate the positions, points were marked in a reticular pattern. The symbols drawn on the pictures are the measured points for Fig. 8. The framed area in (a) is the area shown in Figs. 5 and 6.

were larger than those of CF3. The differences between these and the values with CF1 were especially observable in c_{th} [Fig. 7(b)]. The averages and standard deviations of the magnified area in Fig. 7 were $5.7 \pm 0.6\%$, $4.7 \pm 1.5\%$, and $5.1 \pm 1.2\%$ for melanin with CF1, CF2, and CF3, respectively, and $0.19 \pm 0.05\%$, $0.10 \pm 0.08\%$, and $0.18 \pm 0.05\%$ for hemoglobin with CF1, CF2, and CF3, respectively.

Finally, c_m and c_{th} estimated from different angles at the same site were compared, and the results from a representative example are shown in Fig. 8. The differences between the values

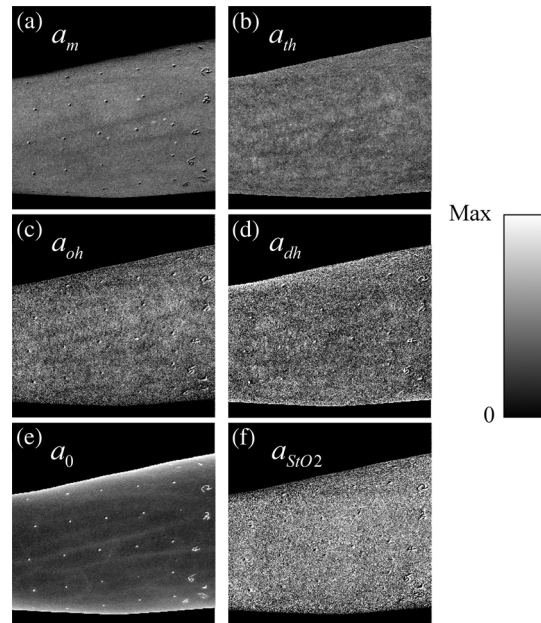


Fig. 5 Representative example of images of the multiple regression coefficients: (a) a_m ; (b) $a_{th} (= a_{oh} + a_{dh})$; (c) a_{oh} ; (d) a_{dh} ; (e) a_0 ; and (f) $a_{SiO_2} (= a_{oh}/a_{th})$. The area of the images is the area surrounded by a border in Fig. 4(a). The background is masked in black. The value of each regression coefficient corresponds to the brightness. The lower limit is zero for all images, and the upper limit ("Max") is 5×10^{-4} for a_m , 4×10^{-6} for a_{th} , 1×10^{-6} for a_{oh} , 1×10^{-6} for a_{dh} , 1 for a_0 , and 100% for a_{SiO_2} . The reticular pattern is made up of points marked on the skin, and it can be clearly seen in (e).

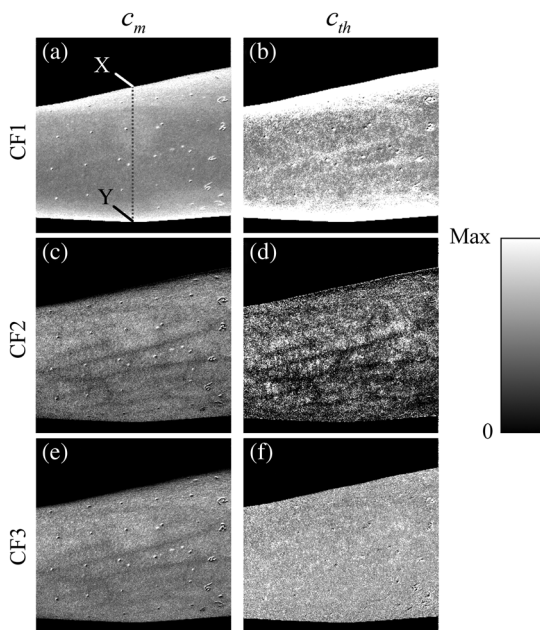


Fig. 6 Estimated c_m and c_{th} with each CF. (a)–(b) with CF1: (a) c_m and (b) c_{th} ; (c)–(d) with CF2: (c) c_m and (d) c_{th} ; (e)–(f) with CF3: (e) c_m and (f) c_{th} . The value of each estimated concentration corresponds to the brightness; the lower limit is zero for all images, and the upper limit (“Max”) is 10% and 0.25% for the images of c_m and c_{th} , respectively. The dotted line and the characters “X” and “Y” in (a) represent the cross-section and ends represented in Fig. 7. The background is masked in black. The reticular pattern is made up of points marked on the skin.

of different angles at each position with CF3 were smaller than those with CF1. The values of σ for the representative example for melanin and hemoglobin (Fig. 8) were, respectively, 1.8% and 0.15% for CF1, 0.3% and 0.02% for CF2, and 0.3% and 0.01% for CF3. The values of σ for melanin and hemoglobin for all sites and all subjects were, respectively, 1.3% and 0.15% for CF1, 0.4% and 0.02% for CF2, and 0.3% and 0.02% for CF3. Figure 9 shows a plot of c_m and c_{th} for all subjects and all points for CF3.

4 Discussion

Under the condition that the forearm was set horizontally and the lights were set at the left and right sides of the camera,

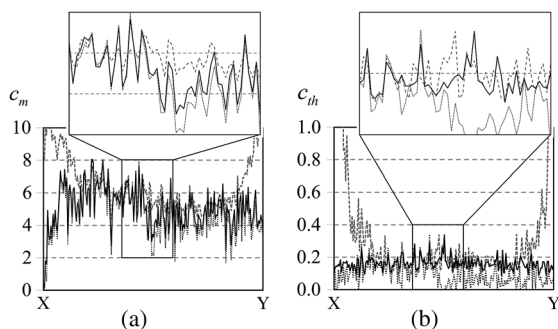


Fig. 7 Cross-sections of the estimated (a) c_m and (b) c_{th} , with CF1, CF2, and CF3. CF1: gray broken lines, CF2: dotted lines, CF3: solid black lines. The plots shown above are the magnified figures of the framed areas. The cross-sections were taken along the dotted lines in Fig. 6(a), and the sides X and Y correspond to the positions noted in Fig. 6(a). The unit of the vertical axes is %.

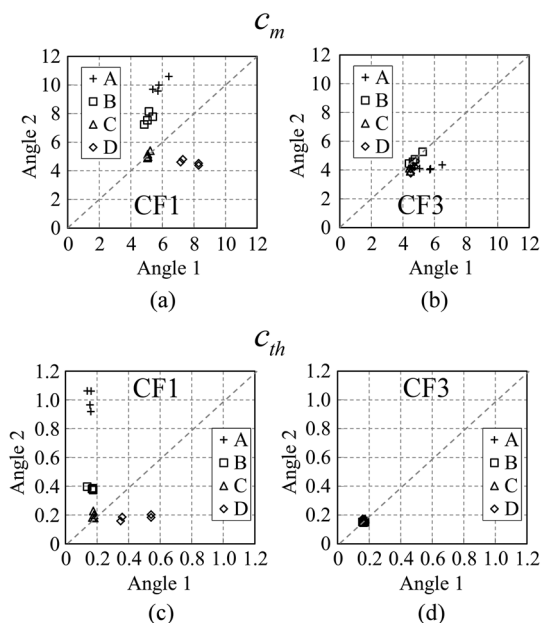


Fig. 8 Correlation between the estimates from different angles (angles 1 and 2) of the melanin and the hemoglobin concentrations at each position of the representative example (same subject as in Fig. 4). (a)–(b): c_m calculated with (a) CF1 and (b) CF3; (c)–(d): c_{th} calculated with (c) CF1 and (d) CF3. The symbols and legend (A to D) are the same as those used in Fig. 4. The unit of the horizontal and vertical axes is %.

the incident angle at the upper and lower sides were greater than that at the center. Therefore, the irradiance at the surface became smaller. As we expected (see Sec. 2.3), the shading effect appeared in the a_0 image [Fig. 5(e)], and became greater at the fringe. As a consequence, with CF1 [Figs. 6(a) and 6(b)], since the formula contains a_0 [Fig. 5(e)], the effect of the shading can be seen in the estimation of chromophore concentrations. This tendency seems to be larger for hemoglobin than for melanin. With CF3 [Figs. 6(e) and 6(f)], which does not contain a_0 , the artifact is hardly seen, as expected. The improvement is shown more clearly in Fig. 8. Each position on the subject should have the same chromophore concentrations even if the measurement angle is changed. Thus the points plotted in Fig. 8 should be on the line $x = y$. Obviously, the points plotted for CF3 were closer to $x = y$ than those for CF1, which were quantified with σ . From these results, we conclude that the

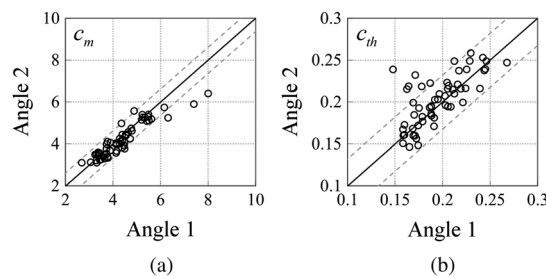


Fig. 9 Correlation between the estimates from different angles (angles 1 and 2) of the melanin and the hemoglobin concentrations at each position for all subjects. (a): c_m ; (b): c_{th} calculated with CF3. The diagonal solid line represents $y = x$, and the diagonal gray broken line represents $y = x \pm 1.96\sigma$, which is the 95% confidence interval assuming the V follows a Gaussian distribution. The unit of the horizontal and vertical axes is %.

estimation errors in the chromophore concentrations that are due to the shading-derived error in the reflectance, were greatly reduced by the proposed approach. With CF3, the σ were 0.3% and 0.02% for c_m and c_{th} , and the ranges of c_m and c_{th} were 3% to 6% and 0.15 to 0.25%, respectively (Fig. 9), which demonstrates that the ratio of the error to the chromophore concentrations is about 10%.

Near the center, where irradiance was evaluated correctly, CF3 estimated the same values, on average, as did CF1 (Fig. 7). In other words, CF3 is as accurate as CF1 when there is less of an effect of shading. Furthermore, the values are within the expected ranges of concentration: c_m , c_{th} , and a_{StO_2} for the representative example were $5.0 \pm 0.7\%$, $0.17 \pm 0.01\%$, and $55 \pm 5\%$, respectively, which agrees with the average values for Japanese subjects as reported in the literature.^{1,22}

In the case of CF2 [Figs. 6(c) and 6(d)], although the shading effect was suppressed, the fluctuation was large. Moreover, the average value is very different from the value with CF1 near the center (Fig. 7). This tendency was notable for c_{th} . This probably came from the error between the expected and estimated chromophore concentrations, which can be seen in Figs. 3(c) and 3(d).

Although in Sec. 2.2, we assumed Lambertian reflection for the angular dependency of reflection from skin as a precondition of the constancy of reflectance with varying outgoing angles, this precondition can be loosened. Lambertian reflection proved to be an inaccurate approximation for several real-world objects.²⁴ However, in the proposed method, to the extent that the angular dependency of the reflected light is proportional between wavelengths, the chromophore concentrations will not be affected by the viewing angle. This is because the multiplication of the reflectance by an independent factor of the wavelength will be included in a_0 in the same way that the shading effect is included in a_0 . From the fact that the variation from the center to the fringe does not explicitly appear in the multiple regression coefficients other than a_0 (Fig. 5), we infer that the loosened precondition is almost true when the viewing angle increases from the center to the fringe, as does the incident angle. Nonetheless, the penetration depth seems dependent in some way besides the shading effect on the incident angle and viewing angles. At the very edge of the forearm, a_{oh} and a_{dh} became slightly smaller and larger, respectively [Figs. 5(c) and (d)], which can be explained by a shallower penetration depth with a larger incident angle. The oxygen saturation in a shallower region is expected to be lower than that in a deeper region,²⁵ which is the trend seen in the derived images.

There are some side effects from removing a_0 from the CFs, and these should be improved. First, although the fluctuations with CF3 were smaller than those with CF2, they were still larger than those with CF1 (Figs. 6 and 7). We tried increasing the maximum degree of CF3 from two to three, but the fluctuations did not improve (not shown). The fluctuations are due directly to a_{oh} and a_{dh} , but did not appear in a_{th} [Fig. 5(b)]. This indicates that the noise in a_{oh} and a_{dh} should be removed in order to reduce the noise in c_{th} . Next, the melanin images from CF3 show what seem to be veins [Fig. 6(e)]. This comes from the a_m image [Fig. 5(a)], and the compensation did not seem to work well without a_0 . Although the average values for CF3 were the same as those for CF1 (Fig. 7), this can create a serious problem in visual understanding. To reduce these problems, although the regression coefficients for the

MRA1 will be converted to chromophore concentrations with CFs, maximizing the accuracy of MRA1 may be effective in terms of the propagation of errors. This means that the more linear the relationship between the regression coefficients of MRA1 and the respective chromophore concentrations, the smaller the estimation error will become. Therefore, for MRA1, employing the modified B–L method instead of the simple B–L method may be effective, because this will improve the correlation between the concentration and the respective regression coefficients of MRA1.

This technique for reducing the shading-derived error does not require any measurements or assumptions about the shape of the subjects and has no limitations as to skin type. In addition, the method is robust against the angular distribution of the reflected light, as discussed in the previous paragraph. However, the method as a whole has inherited some limitations from the base method. First, the estimated chromophore concentrations depend on the optical parameters and geometries used in the MCS. The thicknesses and scattering coefficients of the epidermis and dermis layer can vary with the individual, the site, and the condition of the skin (e.g., water content). Second, an adequate amount of light should be reflected from the dermis for a precise evaluation of the chromophore concentrations. In the case of darker skin, light is strongly absorbed in the epidermis, and the intensity of the light that reaches the dermis is weak. As a consequence, the error in the estimation of the chromophore concentration, especially of oxygenated and deoxygenated hemoglobin, will be larger than that for lighter skin.

In the case of oily skin, the specular reflection is stronger than that of nonoily skin, but this was corrected by using a polarizer in our measuring system. However, the amount of sebum will affect the scattering power of the epidermis, and thus it will also affect the estimated chromophore concentration. The existence of sebum is expected to decrease the scattering power of the surface of the epidermis and thus increase the penetration depth. This may result in an overestimation of the chromophores.

This method is very useful for the diagnoses of skin spots or lesions, especially when they are so large that the surface curvature becomes non-negligible; an example of this is a port-wine stain.²⁶ Also, in aesthetic evaluations in dermatology and cosmetology, evaluations of each body part (especially the face) as a whole are important.²⁷ The robustness of this method against fluctuations in the intensity of the light source provide a practical advantage. In practical applications, the intensity of the light source is sometime not stable; for example, when using a flashbulb. However, to the extent that the spectrum of the light source is proportional, the derived chromophore concentrations will not be affected, since the effect is gathered into a_0 in MRA1. This method is not limited to imaging; it can also be used for point measurements when the stability of the light source intensity cannot be guaranteed. On the other hand, the method cannot be applied when wavelength-dependent information cannot be utilized, such as for the derivation of the absorption and reduced scattering coefficient μ_a and μ'_s .^{16,28} In this case, the effect of shading will also cause errors in the estimated concentrations of chromophores.

5 Conclusion

In this article, we presented a method for quantitative evaluation of skin chromophores over wide regions. We achieved the reduction of shading-derived artifact by eliminating the constant

term of the B–L method in the conversion of the regression coefficients to concentrations. This method is robust to errors in estimating the irradiance and also accounts for the scattering effect. Measurements of a forearm confirmed that, by optimizing the CF, the proposed approach can dramatically reduce the shading-derived artifacts and fully account for the scattering effect. The proposed approach will enable more accurate imaging of large areas, such as whole arms, hands, faces, or legs. Although the method has problems with noise and artifacts, these can be overcome by applying the modified B–L method to MRA1. This issue should be further investigated.

References

- I. Nishidate, Y. Aizu, and H. Mishina, "Estimation of melanin and hemoglobin in skin tissue using multiple regression analysis aided by Monte Carlo simulation," *J. Biomed. Opt.* **9**(4), 700–710 (2004).
- S. Yamamoto et al., "Optical path-length matrix method for estimating skin spectrum," *Opt. Rev.* **19**(6), 361–365 (2012).
- J. B. Dawson et al., "A theoretical and experimental study of light absorption and scattering by in vivo skin," *Phys. Med. Biol.* **25**(4), 695–709 (1980).
- M. Shimada et al., "Explanation of human skin color by multiple linear regression analysis based on the modified Lambert-Beer law," *Opt. Rev.* **7**(4), 348–352 (2000).
- P. Väliuo et al., "New closed-form approximation for skin chromophore mapping," *J. Biomed. Opt.* **16**(4), 046012 (2011).
- T. Maeda et al., "Monte Carlo simulation of spectral reflectance using a multilayered skin tissue model," *Opt. Rev.* **17**(3), 223–229 (2010).
- S. L. Jacques, R. Samatham, and N. Choudhury, "Rapid spectral analysis for spectral imaging," *Biomed. Opt. Express* **1**(1), 157–164 (2010).
- E. Claridge et al., "From colour to tissue histology: physics-based interpretation of images of pigmented skin lesions," *Med. Image Anal.* **7**(4), 489–502 (2003).
- I. Nishidate et al., "Noninvasive spectral imaging of skin chromophores based on multiple regression analysis aided by Monte Carlo simulation," *Opt. Lett.* **36**(16), 3239–3241 (2011).
- N. Tsumura et al., "Image-based skin color and texture analysis/synthesis by extracting hemoglobin and melanin information in the skin," *ACM Trans. Graphics* **22**(3), 770–779 (2003).
- S. Prigent et al., "Multi-spectral image analysis for skin pigmentation classification," in *2010 17th IEEE Int. Conf. Image Process. (ICIP)*, Hong Kong, pp. 3641–3644 (2010).
- J. M. Kainerstorfer et al., "Direct curvature correction for noncontact imaging modalities applied to multispectral imaging," *J. Biomed. Opt.* **15**(4), 046013 (2010).
- J. Sun and M. Smith, "Multidimensional imaging for skin tissue surface characterization," *Comput. Ind.* **64**(9), 1383–1389 (2013).
- K. Uludag et al., "Cross talk in the Lambert-Beer calculation for near-infrared wavelengths estimated by Monte Carlo simulations," *J. Biomed. Opt.* **7**(1), 51–59 (2002).
- N. Okui and E. Okada, "Wavelength dependence of crosstalk in dual-wavelength measurement of oxy- and deoxy-hemoglobin," *J. Biomed. Opt.* **10**(1), 011015 (2005).
- T. T. A. Nguyen et al., "Three-dimensional phantoms for curvature correction in spatial frequency domain imaging," *Biomed. Opt. Express* **3**(6), 1200–1214 (2012).
- L. H. Wang, S. L. Jacques, and L. Q. Zheng, "MCML—Monte Carlo modeling of light transport in multi-layered tissues," *Comput. Methods Programs Biomed.* **47**(2), 131–146 (1995).
- S. L. Jacques and D. J. McAuliffe, "The melanosome: threshold temperature for explosive vaporization and internal absorption coefficient during pulsed laser irradiation," *Photochem. Photobiol.* **53**(6), 769–775 (1991).
- S. A. Prahl, "Optical absorption of hemoglobin," <http://omlc.ogi.edu/spectra/hemoglobin/index.html> (1999).
- S. L. Jacques, "Origins of tissue optical properties in the UVA, visible, and NIR regions," pp. 364–369, Optical Society of America (OSA), Washington, DC (1996).
- M. J. C. van Gemert et al., "Skin optics," *IEEE Trans. Biomed. Eng.* **36**(12), 1146–1154 (1989).
- S. L. Jacques, "Skin optics summary," <http://omlc.ogi.edu/news/jan98/skinoptics.html> OMLC news Jan 1998 (1998).
- I. Nishidate, Y. Aizu, and H. Mishina, "Estimation of absorbing components in a local layer embedded in the turbid media on the basis of visible to near-infrared (VIS-NIR) reflectance spectra," *Opt. Rev.* **10**(5), 427–435 (2003).
- M. Oren and S. K. Nayer, "Generalization of Lambert's reflectance model," in *SIGGRAPH '94 Proc. 21st Ann. Conf. Comput. Graphics Interact. Tech.*, pp. 239–246, ACM, New York (1994).
- T. Forst et al., "Reliability of lightguide spectrophotometry (O2C®) for the investigation of skin tissue microvascular blood flow and tissue oxygen supply in diabetic and nondiabetic subjects," *J. Diabetes Sci. Technol.* **2**(6), 1151–1156 (2008).
- B. Jung et al., "Characterization of port wine stain skin erythema and melanin content using cross-polarized diffuse reflectance imaging," *Lasers Surg. Med.* **34**(2), 174–181 (2004).
- N. Ojima et al., "Application of image-based skin chromophore analysis to cosmetics," *J. Imaging Sci. Technol.* **48**(3), 222–226, 236–238 (2004).
- S. Gioux et al., "Three-dimensional surface profile intensity correction for spatially modulated imaging," *J. Biomed. Opt.* **14**(3), 034045 (2009).

Biographies of the authors are not available.